Extraction of PAHs in DP: PAHs in water were extracted by solid phase extraction using a C18 cartridge (Waters Sep-Pak C-18 Cartridge). The cartridges were preconditioned with 5 mL methanol and by 5 mL distilled water. After preconditioning, water samples were applied to the cartridges. The flow rate of sample through the cartridge was 10 mL/min. After all samples were percolated, the cartridges were dried under vacuum condition. PAHs in the cartridge were eluted with 15 mL of dichloromethane (Kiss et al., 1996). Surrogate recovery standards (Nap-d_8, Ace-d_{10}, Phe-d_{10}, Pyr-d_{10} and BaP-d_{12}) were added to the cartridge just before the elution. PAHs in the extracts were concentrated by rotary evaporation to dryness and then the residue was dissolved in 1 mL hexane for the clean-up procedure.

Extraction of PAHs in PP: the glass fiber filters were soaked in a 40 mL mixture of benzene and ethanol (3:1, v/v). Surrogate recovery standards (Nap-d_8, Ace-d_{10}, Phe-d_{10}, Pyr-d_{10} and BaP-d_{12}) were added to the sample just before the extraction. The mixtures were extracted in an ultrasonic bath (NSD Japan, US-106, 38 kHz, 300 W) for 30 min. Extracts were then filtered. The extraction was repeated once without adding surrogate recovery standard. PAHs in the extracts were concentrated by rotary evaporation to dryness and then the residue was dissolved in 1 mL hexane for the clean-up procedure.

2.4. Clean-up

After extraction, the samples were cleaned up with a silica gel cartridge (Water Sep-Pak Silica Cartridge). The cartridges were preconditioned with 5 mL of hexane. Samples were applied to the cartridges and the PAHs were eluted with a mixture of hexane and acetone (9:1, v/v). After clean-up, 200 μL DMSO was added PAHs in the extracts were concentrated by rotary evaporation and then the residue was dissolved in 800 μL acetonitrile. An aliquot (20 μL) of the solution was injected into the HPLC.

2.5. HPLC

The HPLC system consisted of two Hitachi L-2130 pumps, a Hitachi degasser, a Hitachi L-2485 fluorescence detector and a Hitachi organizer. The analytical column and guard column were Inertsil ODS-P (4.6 i.d. × 250 mm, 5 μm, GL Sciences) and Inertsil ODS-P (4.0 i.d. × 10 mm, 5 μm, GL Sciences), respectively. Both of the columns were kept at 20 °C. The mobile phase was a mixture of acetonitrile and distilled water set in a linear gradient program. The flow rate of mobile phase was kept at 1.0 mL/min. The sample was detected by the fluorescence detector for which the excitation and emission wavelengths were automatically set by a time program.

Fifteen PAHs from USEPA's 16 priority PAHs list were quantified: the two-ring PAH was Napthalene (Nap); three-ring PAHs were Acenaphtene (Ace), Fluorene (Fle), Anthracene (Ant) and Phenanthrene (Phe); four-ring PAHs were Fluoranthene (Flu), Pyrene (Pyr), benz[a]anthracene (BaA) and Chrysene (Chr); five-ring PAHs were Benzo[b]fluoranthene (BbF), Benzo[k]fluoranthene (BkF), Benzo[a]pyrene (BaP) and Dibenz[a,h]anthracene (DBA); six-ring PAHs were Benzo[ghi]perylene (BgPe) and Indeno[1,2,3-cd]pyrene (IDP). Nap and Phe could not be quantified because of too low recovery rate and poor resolution in chromatography results, respectively.

The wavelengths of fluorescence were set according to the optimization excitation and emission of each PAH. The excitation and emission wavelengths were set at 280 and 340 nm for Nap, Ace, Fle, and Phe; 250 and 400 nm for Ant; 286 and 433 nm for Flu; 331 and 392 nm for Pyr; 264 and 407 nm for BaA, Chr, BbF, BkF, BaP, DBA, and BgPe; and 294 and 482 nm for IDP, respectively.

3. Results and discussion

3.1. Distribution of PAHs in the surface waters of the Japan Sea

Table 1 shows the concentrations of the 13 PAHs identified in the surface waters of the Japan Sea. The total concentrations of the 13 PAHs ranged from 7.4 to 10.2 ng/L with a mean concentration of 7.9 ng/L. These data are significantly lower as compared with those of the studies for the other seas in the Far East Asia, e.g., for the Western Taiwan Strait connecting the East China Sea and the South China Sea the total concentrations of PAHs varied from 23.3 to 70.9 ng/L (Wu et al., 2011) and for the East China Sea—70.22–120.29 ng/L (Ren et al., 2010). Excepting stations A1 and B1, the values of the total concentration of PAHs were similar for all other stations.

The highest concentrations (about 10 ng/L) were observed at stations A1 (the northernmost station of the cruise) and B1 (the station of the cruise closest to Japan). High concentration of PAHs at station A1 may be related to the proximity of the Amur River waters, which are probably indicated lower salinity of surface seawater at this station (32.398 psu). As for high concentration of PAHs at station B1 it may be associated with the Tsushima Current from East China Sea. The surface waters of the warm Tsushima Current spread over the southern Japan Sea to the Subpolar Front (approximately at 40°N) and converge around the western side of the Tsugaru Strait. Then current flows out through

Table 1
Concentrations of PAHs in the surface samples of the Japan Sea. Cruise Lav-51.

PAHs	DP (ng/L)				PP (ng/L)					Total (DP + PP) (ng/L)		
	Max.	Min.	Mean	Std. dev.	Max.	Min.	Mean	Std. dev.	Max.	Min.	Mean	Std. dev.
Ace	1.0	0.8	0.9	0.09	1.0	0.6	0.7	0.13	1.92	1.48	1.52	0.15
Fle	2.6	1.8	2.1	0.24	0.64	0.35	0.42	0.08	3.13	2.25	2.39	0.28
Ant	0.50	0.26	0.34	0.06	0.093	0.051	0.064	0.011	0.59	0.31	0.38	0.07
Flu	0.90	0.24	0.63	0.16	0.69	0.12	0.31	0.15	1.32	0.59	0.90	0.18
Pyr	2.3	0.8	1.3	0.35	1.10	0.17	0.60	0.26	3.17	1.36	1.80	0.5
BaA	0.16	0.03	0.07	0.035	0.083	0.029	0.048	0.017	0.19	0.07	0.11	0.037
Chr	0.078	0.022	0.036	0.014	0.292	0.036	0.09	0.069	0.32	0.06	0.12	0.07
BbF	0.065	0.025	0.044	0.012	0.11	0.07	0.09	0.012	0.18	0.11	0.13	0.02
BkF	0.016	0.010	0.012	0.002	0.055	0.035	0.043	0.005	0.068	0.048	0.054	0.006
BaP	0.027	0.007	0.016	0.006	0.052	0.024	0.037	0.008	0.072	0.035	0.051	0.011
DBA	0.063	0.023	0.039	0.011	0.13	0.07	0.09	0.018	0.18	0.09	0.12	0.023
BgPe	0.063	0.030	0.042	0.009	0.17	0.07	0.11	0.025	0.21	0.11	0.15	0.026
IDP	0.051	0.008	0.027	0.012	0.29	0.03	0.13	0.079	0.333	0.032	0.151	0.08
∑PAHs	6.521	4.758	5.605	0.882	3.725	2.126	2.731	0.807	10.246	7.387	7.880	1.681

the Tsugaru and Soya Straits, and the rest trends northward (Kosuke et al., 2005). Therefore the surface waters of the East-China Sea can be considered as source of PAHs for the Japan Sea.

Table 1 and Fig. 2 show the concentrations of the 13 PAHs in DP and PP ranged from 4.8 to 6.5 ng/L (mean—5.6 ng/L) and 2.1 to 3.7 ng/L (mean—2.7 ng/L), respectively. In the both phases, DP and PP, 3-ring and 4-ring PAHs were dominant. But concentrations of PAHs with 3-ring and 4-ring (excepted Chr) were higher in DP than in PP. While concentrations of Chr and 5,6-rings PAHs were 2–5 times higher in PP than in DP. These results indicate that DP and PP contained 67% and 33% of the total PAHs, respectively. Similarly, in the atmosphere low molecular weight PAHs are mainly in the gas phase, while high molecular weight species are in particulate phase (Dickhut et al., 2000). For the Mediterranean Sea, which similar to the Japan Sea, due to connecting with adjacent basins by straits, the concentrations of PAHs in DP ranged from 0.4 (in the open sea) to 2.2 ng/L (in the estuaries). The concentrations of PAHs in PP ranged from 0.3 to 1.1 ng/L accounting for 30–40% of total PAHs (Dachs et al., 1997). This correlation agrees with our data. The higher concentrations of PAHs in this investigation can be explained that the sampling for the Mediterranean Sea's study was conducted in 1993 and 11 PAHs were analyzed.

3.2. PAHs ratios as markers of PAHs contamination

Different genetic sources of PAHs have the various ratios between the individual compounds themselves. Therefore these ratios have been selected as markers to determine the sources of pollution of ecosystems by PAHs. Yunker et al. (2002) use PAH isomer pairs ratios Ant/(Phe+Ant), Flu/(Flu+Py), BaA/(BaA+Chr) and IDP/(IDP+BgPe) to elucidate possible sources of PAHs in marine environment. They proposed that for IDP/(IDP+BgPe), a ratio <0.2 probably implies petroleum (petrogenic source), 0.2–0.5 implies petroleum combustion (liquid fossil fuels combustion), and >0.5 implies grass, wood or coal combustion; for Flu/(Flu+Pyr) the petroleum boundary ratio appears close to 0.4, and the ratio between 0.4 and 0.5 is characteristic of petroleum combustion, whereas a ratio >0.5 is characteristic of implies grass, wood or coal combustion. Similarly, the BaA/(BaA+Chr) ratio of less than 0.2 implies the petroleum input, between 0.2 and 0.35 suggests liquid fossil fuel combustion and more than 0.5 infers grass, wood and coal combustion (Wu et al., 2011). As shown in Fig. 3A and B, the ratios IDP/(IDP+BgPe) were ranged from 0.2 to 0.8, and the values in PP were a little higher than those in DP. On the contrary the values of BaA/(BaA+Chr) ratios in DP were a little higher than those in PP and were ranged from 0.4 to 0.9 for DP and from 0.2 to 0.6 for PP (Fig. 3C and D). Flu/(Flu+Pyr) ratios were mostly found in the range from 0.2 to 0.4; the values in PP and DP are very similar (Fig. 3A–D). This suggests that PAHs mainly descended from the mixed sources both with the inputs from petrogenic and pyrolytic origins.

3.3. Vertical distribution of PAHs at the station D1

The main feature of hydrophysical characteristics determining the vertical structure of the Japan Sea is that all of the subtropical water from about 300 m to the bottom and all of the subpolar water in the Japan Sea is very ventilated north of the Subpolar Front. All of this subpolar-ventilated water can be referred to as Japan Sea Proper Water, once thought to be a nearly homogenous water mass (Talley et al., 2006). Station D1 is located about 50 km

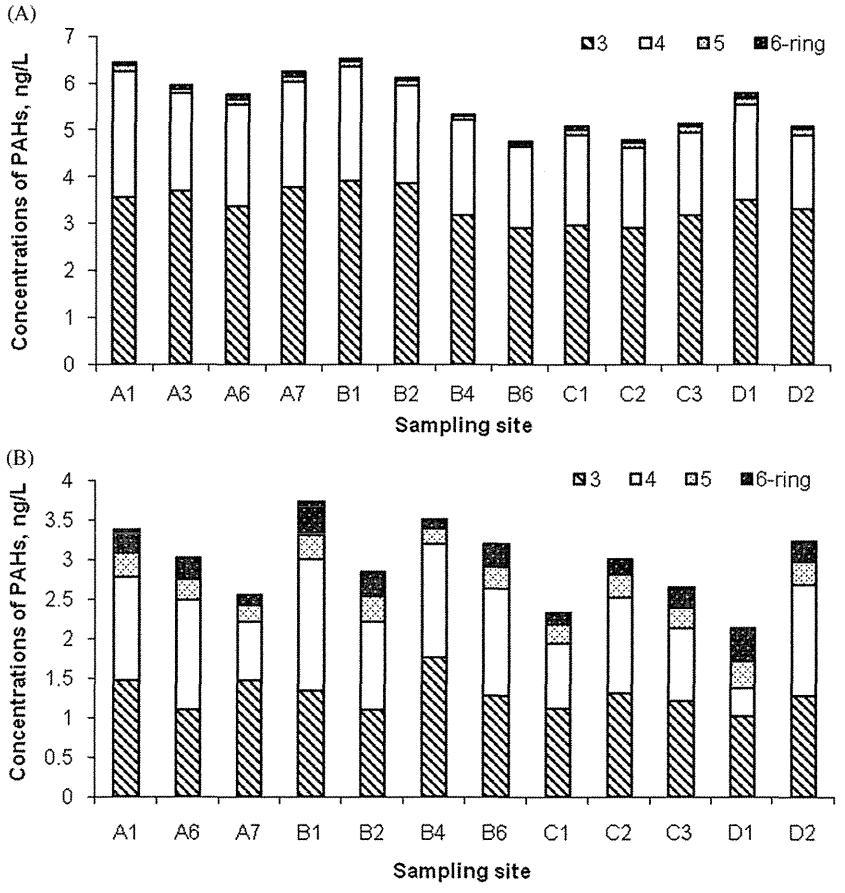

Fig. 2. Concentrations of PAHs in the surface seawater in DP (A) and PP (B).

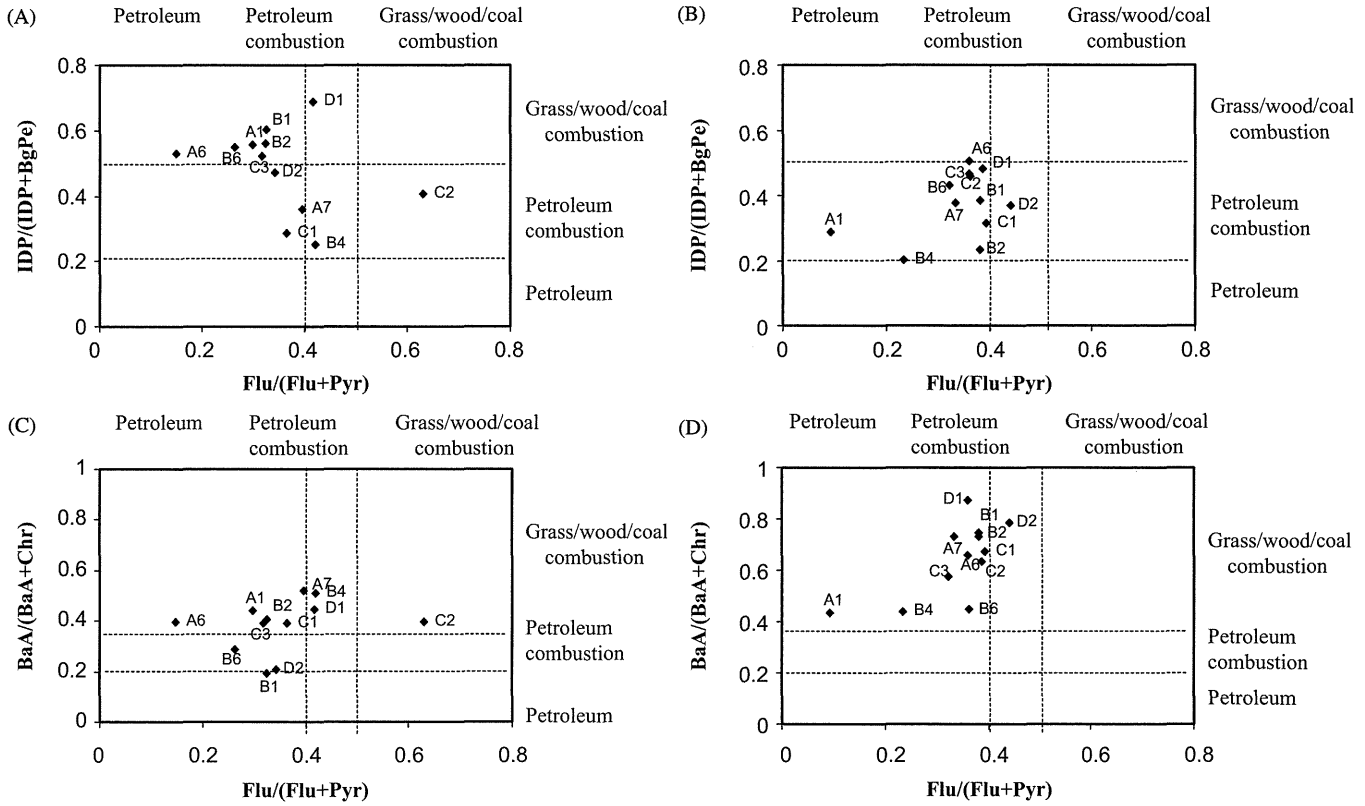

Fig. 3. Ratios of IDP/(IDP+BgPe) vs. Flu/(Flu+Pyr) in PP (a) and DP (b); BaA/(BaA+Chr) vs. Flu/(Flu+Pyr) in PP (c) and DP (d) in the stations of the cruise Lav-51.

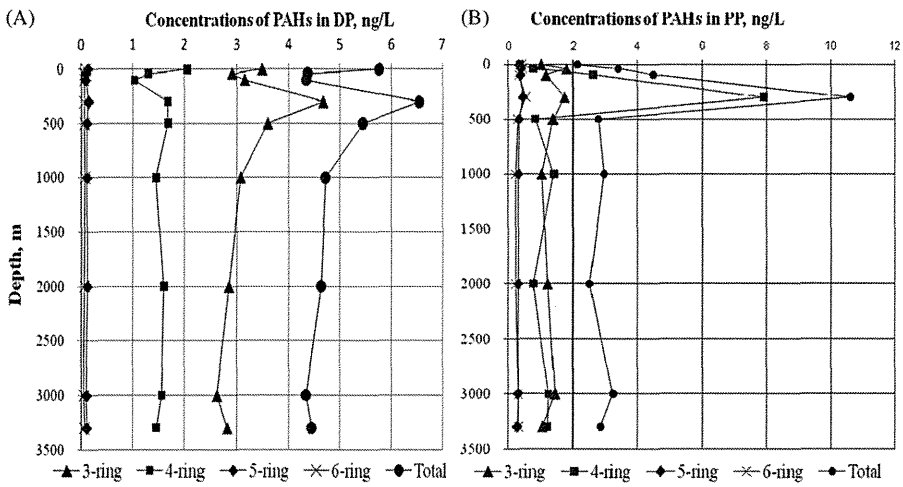

Fig. 4. Vertical distribution of PAHs in DP (a) and PP (b) at the station D1.

far from northern edge of the Subpolar Front. This area is characterized as relatively high productive unit. Vertical distribution of PAHs in PP and DP is almost homogenous below 500 m (Fig. 4). The maximum concentrations of PAHs in DP and PP were detected on the sea surface and at a depth of 300 m. The high concentrations of PAHs for the sea surface indicate the main source of PAHs is the solid particles of the atmosphere (aerosols). Sufficiently high concentrations of PAHs for greater depths lead us to the same conclusion. We assume the basic mechanism of penetration of PAHs in the deep horizons of the sea is the settling of solid particles with adsorbed PAHs. Otherwise, the penetration of these compounds in the intermediate and deep waters of the sea only by the mechanism of turbulent diffusion would take several decades, during which low molecular PAHs with a half-life of several tens of days are destroyed. During the settling of the solid particles, PAHs partially transfers from the particulate phase to the dissolved phase. The rate of deposition of particles varies widely from a few meters to several hundred meters per day (Burd and Jackson, 2009). A depth of 300 m showed the highest concentrations of PAHs. Particulate phase on this depth contains a high concentration of Pyr (4 ng/L). As observed zooplankton fecal pellets are important vector of vertical flux of PAHs (Lipiatou et al., 1993). In an earlier authors have found the plankton samples contain high concentrations of Pyr and Flu (Lipiatou and Saliot, 1992). Therefore we suggest the relationship between the maximum of the Pyr-concentration at the depth 300 m and zooplankton fecal pellets.

4. Conclusions

This investigation first provides the data of PAHs spatial distribution in the northwestern part of the Japan Sea and contributes to the present status of PAHs contamination in studied region.

Thirteen PAHs were quantitatively analyzed in this study. The values of total PAHs concentration in the Japan Sea were similar for surface seawater at all stations (excepting stations A1 and B1) and were ranged from 7.4 to 10.2 ng/L with a mean concentration of 7.9 ng/L. The level of PAHs contamination was founded lower in comparison with others seas of the Far East Asia.

Data PAHs isomer pair ratios Flu/(Flu+Py), BaA/(BaA+Chr) and IDP/(IDP+BgPe) suggest that PAHs mainly descended from the mixed sources both with the inputs from petrogenic and pyrolytic origins.

Vertical distribution of total PAHs was detected maxima on the sea surface and depth of 300 m. We assume the former originate from atmosphere and the later relate with zooplankton fecal pellets.

Acknowledgments

This research was partially supported by the grant # 12-I-P30-07 from Presidium of Far Eastern Branch Russian Academy of Science. Also the authors have greatly appreciated to reviewer Dr. Ying Li and anonymous reviewer of this paper. Their reasonable remarks and comments seriously helped to improve this paper quality and obtain its final form.

Also this work was supported by the Grant for young researchers of Japan-Russia Youth Exchange (JREX, Tokyo, Japan).

References

Burd, A.B., Jackson, G.A., 2009. Particle aggregation. Annu. Rev. Mar. Sci. 1, 65–90.

D'Adamo, R., Pelosi, S., Trotta, P., Sansone, G., 1997. Bioaccumulation and biomagnification of polycyclic aromatic hydrocarbons in aquatic organisms. Mar. Chem. 56 (1–2), 45–49.

Dachs, J., Bayona, J.M., Raoux, C., Albaiges, J., 1997. Spatial, vertical distribution and budget of polycyclic aromatic hydrocarbons in the western Mediterranean seawater. Environ. Sci. Technol. 31, 682–688.

Dickhut, R.M., Canuel, E.A., Gustafson, K.E., Liu, K., Arzayus, K.M., Walker, S.E., Edgecombe, G., Gaylor, M.O., Macdonald, E.H., 2000. Automotive sources of carcinogenic PAHs associated with particulate matter in the Chesapeake Bay region. Environ. Sci. Technol. 34, 4635–4640.

Ding, Xiang, Wang, X.-M., Xie, Z.-Q., Xiang, C.-H., Mai, B.-X., Sun, L.-G., Zheng, M., Sheng, G.-Y., Fu, J.-M., Poshel, U., 2007. Atmospheric polycyclic hydrocarbons observed over the North Pacific Ocean and the Arctic area: spatial distribution and source identification. Atmos. Environ. 41, 2061–2072.

Dobrovol'skii, A.D., Zalogin, B.S., 1982. Seas of the USSR. Moscow State University, Moscow 192 p.

Feng, J., Hu, M., Chan, C.K., Lau, P.S., Fang, M., He, L., Tang, X., 2006. A comparative study of the organic matter in PM2.5 from three Chinese megacities in three different climatic zones. Atmos. Environ. 40, 3983–3994.

Haritash, A.K., Kaushik, C.P., 2009. Biodegradation aspects of Polycyclic Aromatic Hydrocarbons (PAHs): a review. J. Hazard. Mater. 169, 1–15.

Hayakawa, K., Tang, N., Kameda, T., Toriba, A., 2007. Atmospheric behaviors of polycyclic aromatic hydrocarbons and nitropolycyclic aromatic hydrocarbons in East Asia. Asian J. Atmos. Environ. 1 (1), 19–27.

Huang, D., Peng, P., Xu, Y., Deng, Y., Deng, H., 2009. Distribution and deposition of polycyclic aromatic hydrocarbons in precipitation in Guangzhou, South China. J. Environ. Sci. 21, 654–660.

Johnsen, A.R., Wick, L.Y., Harms, H., 2005. Principles of microbial PAH-degradation in soil. Environ. Pollut. 133, 71–84.

Kaneyasu, N., Takeuchi, K., Hayashi, M., Fujita, S., Uno, I., Sasaki, H., 2000. Outflow patterns of pollutants from East Asia to the North Pacific in the winter monsoon. J. Geophys. Res. 105, 17361–17377.

Kiss, G., Varga-Puchony, Z., Hlavay, J., 1996. Determination of polycyclic aromatic hydrocarbons in precipitation using solid-phase extraction and column liquid chromatography. J. Chromatogr. A 725 (2), 261–272.

Kosuke, M., Takeshi, M., Senju, T., 2005. Seasonal/spatial variations of the near-inertial oscillations in the deep water of the Japan Sea. J. Oceanogr. 61 (4), 761–773.

Lipiatou, E., Saliot, A., 1991. Fluxes and transport of anthropogenic and natural polycyclic aromatic hydrocarbons in the western Mediterranean Sea. Mar. Chem. 32, 51–71.

Lipiatou, E., Saliot, A., 1992. Biogenic aromatic hydrocarbon geochemistry in the rhone river delta and in surface sediments from the open North-western Mediterranean Sea. Estuarine Coastal Shelf Sci. 34, 515–531.

Lipiatou, E., Marty, J.-C., Saliot, A., 1993. Sediment trap fluxes of polycyclic aromatic hydrocarbons in the Mediterranean Sea. Mar. Chem. 44, 43–54.

McGowin, A.E., 2006. Polycyclic aromatic hydrocarbons. In: Nollet, L.M.L. (Ed.), Chromatographic Analysis of the Environment, third ed. CRC Press Taylor & Francis Group, pp. 556–616.

Nemirovskaya, I.A., 2007. Hydrocarbons in water and bottom sediments of a region with continuous petroleum contamination. Geokhimiya 7, 704–717 (in Russian).

Neff, J.M., 2002. Polycyclic aromatic hydrocarbons in the ocean. In: Neff, J.M. (Ed.), Bioaccumulation in Marine Organisms. Elsevier Science, pp. 241–318.

Ogi, M., Tachibana, Y., Nishio, F., Danchenkov, M.A., 2001. Does the fresh water supply from the Amur River flowing into the Sea of Okhotsk affect sea ice formation? J. Meteorol. Soc. Jpn. 79, 123–129.

Ren, H., Kawagoe, T., Jia, H., Endo, H., Kitazawa, A., Goto, S., Hayashi, T., 2010. Continuous surface seawater surveillance on poly aromatic hydrocarbons (PAHs) and mutagenicity of East and South China Seas. Estuarine Coastal Shelf Sci. 86, 395–400.

Shuttleworth, K.L., Cerniglia, C.E., 1995. Environmental aspects of PAH biodegradation. Appl. Biochem. Biotechnol. 54, 291–302.

Talley, L.D., Min, Dong-Ha, Lobanov, V.B., Luchin, V.A., Ponomarev, V.I., Salyuk, A.N., Shcherbina, A.Ya., Tishchenko, P.Ya., Zhabin, I.A., 2006. Japan/East Sea water masses and their relation to the sea's circulation. Oceanography 19 (3), 32–49.

Tang, N., Hattori, T., Taga, R., Igarashi, K., Yang, X., Toriba, A., Kizu, R., Hayakawa, K., Tamura, K., Kakimoto, H., Mishukov, V.F., 2005. Polycyclic aromatic hydrocarbons and nitropolycyclic aromatic hydrocarbons in urban air particulates and their relationship to emission sources in the Pan-Japan Sea countries. Atmos. Environ. 39, 5817–5826.

WHO, 2000. The World Health Report 2000: Health Systems: Improving Performance. World Health Organization, Geneva.

WHO, 2001. International Programme on Chemical Safety, Environmental Health Criteria 202. Selected Non-heterocyclic Polycyclic Aromatic Hydrocarbons. World Health Organization, Geneva.

Wu, Y.-L., Wang, X.-H., Li, Y.-Y., Hong, H.-S., 2011. Occurrence of polycyclic aromatic hydrocarbons (PAHs) in seawater from the Western Taiwan Strait, China. Mar. Pollut. Bull. 63, 459–463.

Yakunin, L.P., 1978. Distribution of Amur River runoff between mouth's channels. In: Vladivostok, FERHRI Proceedings, vol. 71, pp. 162–168 (in Russian).

Yang, X.-Y., Okada, Y., Tang, N., Matsunaga, S., Kameda, T., Toriba, A., Hayakawa, K., Tamura, K., Lin, J.M., 2007. Long-range transport of polycyclic aromatic hydrocarbons from China to Japan. Atmos. Environ. 41, 2710–2718.

Yunker, M.B., Macdonald, R.W., Vingarzan, R., Mitchell, R.H., Goyette, D., Sylvestre, S., 2002. PAHs in the Fraser River basin: a critical appraisal of PAH ratios as indicators of PAH source and composition. Org. Geochem. 33, 489–515.

[Review]

Biological Effects of Polycyclic Aromatic Hydrocarbon Derivatives

Kanae BEKKI[1], Akira TORIBA[2], Ning TANG[2,3], Takayuki KAMEDA[2] and Kazuichi HAYAKAWA[2]

[1] *Division of Environmental Science and Engineering, Graduate School of Natural Science and Technology, Kanazawa University, Kakumamachi, Kanazawa, Ishikawa 920-1164, Japan*

[2] *Faculty of Pharmaceutical Sciences, Institute of Medical, Pharmaceutical and Health Sciences, Kanazawa University, Kakumamachi, Kanazawa, Ishikawa 920-1164, Japan*

[3] *Hyogo College of Medicine, Mukogawa-cho, Nishinomiya, Hyogo 663-8501, Japan*

Abstract : Polycyclic aromatic hydrocarbons (PAHs) are included in various environmental pollutants such as airborne particles and have been reported to induce a variety of toxic effects. On the other hand, PAH derivatives are generated from PAHs both through chemical reaction in the atmosphere and metabolism in the body. PAH derivatives have become known for their specific toxicities such as estrogenic/antiestrogenic activities and oxidative stress, and correlations between the toxicities and structures of PAH derivatives have been shown in recent studies. These studies are indispensable for demonstrating the health effects of PAH derivatives, since they would contribute to the comprehensive toxicity prediction of many kinds of PAH derivatives.

Key words : PAH derivative, structure activity relationship, estrogenic/antiestrogenic activity, reactive oxygen species.

(Received October 1, 2012, accepted December 25, 2012)

Introduction

An important group of pollutants associated with airborne particulate matter (PM) are polycyclic aromatic hydrocarbons (PAHs), which are constructed of two or more aromatic rings and are produced by incomplete combustion of fossil fuels. PAHs have carcinogenicity and mutagenicity [1], and have been classified according to International Agency for Research for Cancer (IARC) as carcinogenic or probably carcinogenic compounds [2, 3]. PAHs are believed to be the main causal compounds in the health effects of ambient air pollutants. PAHs generate various derivatives both in the atmosphere and in the body. PAH derivatives are becoming known to have particular effects, such as oxidative stress and endocrine disruption. Many studies give information on the possible roles of PAH derivatives in several diseases which have been increasing for several decades worldwide. However, a comprehensive assessment of the toxicities of these compounds is not easy, since numerous PAH derivatives exist in the atmosphere and they have different toxicities.

In recent years, studies of the structure and activity relationship have developed in the study of environmental science. This study can predict the possibility of the toxicities of compounds according to the relationship between chemical three-dimensional (3D) structures, even though the toxicities of their compounds have not been measured. Therefore, an analysis of the structure and activity relationship is a key to know the health risk of numerous compounds in the

Corresponding Author: Kanae BEKKI, Division of Environmental Science and Engineering, Graduate School of Natural Science and Technology, Kanazawa University, Kakumamachi, Kanazawa, Ishikawa 920-1192, Japan. Tel: + 81-76-234-4413, Fax: +81-76-234-4456, E-mail: bekkana1105@gmail.com

atmosphere, including PAH derivatives.

This review provides information mainly about our recent observation assessing the relationship between structural and biological activities of PAH derivatives.

Generation of PAH derivatives

It is well known that PAH derivatives such as hydroxylated PAHs (OHPAHs) and PAH quinones (PAHQs) are generated in the atmosphere through chemical reactions with nitrogen radicals (•NO^3), hydroxide radicals (•OH) and ultraviolet light [4–6]. These PAH derivatives are also generated in the body. After entering the body, PAHs bind to one of the nuclear receptors, the aryl hydrocarbon receptor (AhR), and then induce the cytochrome P450 drug-metabolizing enzymes such as *Cyp1a1*, *Cyp1a2* and *Cyp1b1*, which metabolize PAHs into various PAH derivatives.

Toxicities of PAH derivatives

Concerning the toxicities of PAH derivatives, the mutagenicity induced by nitrated PAHs (NPAHs) has been well known for many years [7]. In recent years, it has been shown that other PAH derivatives also show various toxicities. For instance, PAHQs produce reactive oxygen species (ROS) through redox cycle, leading to ROS-related toxicities, such as physical DNA damage, oxidative stress and cell death [8–10]. The most important information is that PAH derivatives-induced oxidative stress might be involved in various diseases, such as allergic reaction, circulatory organ system disease, infection and aging [11–17]. Cho *et al.* have recently reported that phenanthrenequinone (PQ) induced the recruitment of inflammatory cells, such as eosinophils and neutrophils, into the lung with the lung expression of pro-inflammatory molecules such as interleukin (IL)-5 and eotaxin *in vivo* [19]. PQ also aggravates antigen-related airway inflammation in mice, and PQ has adjuvant activity for antigen-specific immunoglobulin G (IgG), leading to aggravation of antigen-related airway inflammation in mice [20]. Because PQ is a major quinone in diesel exhaust particles (DEP) [18], which have been reported to cause lung inflammatory-related impacts, these reports suggest a key role of PQ in lung diseases by air pollutants.

Interestingly, there are several reports suggesting that PAH derivatives have endocrine disruptor-like activities. DEP extracts including numerous PAH derivatives exhibit estrogenic and/or antiestrogenic activities in human MCF-7 breast cancer cells and recombinant yeast cells [21–23]. These samples also exhibited a significant antiandrogenic effect in PC3/AR human prostate carcinoma cells [24]. Actually, one of the OHPAHs, hydroxyphenanthrene (OHPhe) and hydroxyfluoranthene (OHFrt), constructed with three or four rings, were determined in the DEP extracts as antiandrogenic compounds. Furthermore, strong estrogenic activities of several OHPAH isomers, hydroxybenz[*a*]anthracene (OHBaA) and hydroxychrysene (OHCh), were also detected by screening evaluation using yeast two-hybrid assay [25].

Structure activity relationship of estrogenic/antiestrogenic activity of PAH derivatives

It has gradually become known that the endocrine disruptor-like activities of PAH derivatives are related to their structure. It has been reported theoretically that the common structure of estrogenic compounds is a phenol with a hydrophobic moiety at the *para*-position without a bulky group at the *ortho*-position [26]. This theory could be applied to the activities of PAH derivatives. In our recent study, we investigated whether OHPAHs, PAHQs and PAH ketones (PAHKs) having two to six rings show estrogenic or antiestrogenic activities [25, 27] by using the yeast two-hybrid assay system [28], in order to elucidate the characteristics of PAH derivatives in more detail.

Among the OHPAHs we tested, strong estrogenic activity was observed mainly in OHPAHs having 4 rings. We also observed strong antiestrogenic activity in several OHPAHs having 4 and 5 rings [25]. Because PAHs can't bind to the active site of human estrogen receptor (hER), it is strongly suggested that the hydroxyl modification and its location are key factors for the large difference in estrogenic activities between PAHs and OHPAHs. At this time, relative binding affinity (RBA) is also correlated with estrogenic or antiestrogenic activity [29]. On the other hand, we have found that several PAHQs also showed strong antiestrogenic activities, suggesting that exhibition of

antiestrogenic activity mainly depends on the location of substituted groups rather than on the kinds of functional groups [30].

It has been reported that the phenol group (OH-3) of 17β-estradiol (E_2) makes hydrogen bonds with Glu353 and Arg394 of hER and H_2O and that the alcohol group (OH-17) of E_2 has an affinity for the nitrogen atom of His524 of hER. On the other hand, van der Walls interaction takes place between the benzene ring of E_2 and the benzene ring of Phe404 of the binding site of hER [31, 32]. These reports suggest that 4-ring OHPAHs interact with the binding site of hER, and this binding mechanism depends on the phenol group. Furthermore, several physical parameters, such as the length-to-breadth (L/B) ratios of the rectangular van der Walls plane surrounding each PAH molecule and O-H distance, the distance between the oxygen atom of the phenol group and the hydrogen atom located farthest from the phenol group and partial charge, might be correlated with these binding mechanisms between E_2 and estrogen receptor (ER), showing a correlation with estrogenic/antiestrogenic activities of OHPAHs and PAHQs. Especially, L/B and O-H distance showed an effect on the activity (Fig. 1).

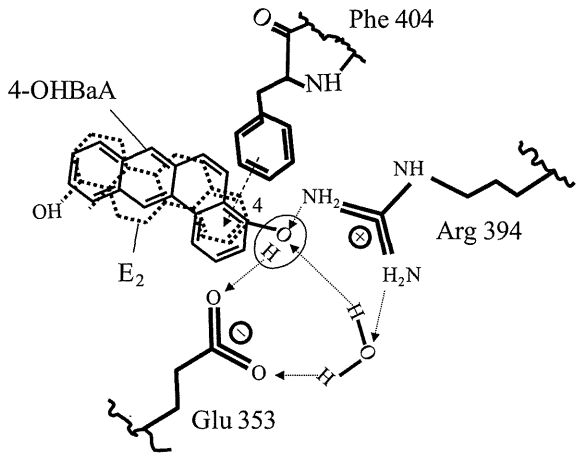

Fig. 1. Speculation of binding of OHPAH to hER.

Furthermore, compounds having a strong affinity to hER, such as E and diethylstilbestrol (DES), have two hydroxyl groups with the appropriate O-O distance [31]. The L/B ratios of E_2 and DES were 1.545 and 1.515, respectively. These L/B ratios and O-O distances were close to the value of L/B ratios and O-H distances of the above strongly estrogenic OHPAHs in the small circle area (Fig. 2). The area of the L/B ratio and O-H distance of the strongly antiestrogenic OHPAHs was much larger than that of the strongly estrogenic OHPAHs described above. Although it is unclear why 9-OHBaA was an exception, this result suggests that antagonistic OHPAHs can exhibit activity even when they bind to sites other than the active site of hER.

These facts suggest that the activities of OHPAHs and PAHQs can be roughly predicted from their physical parameters, although differentiation between agonistic and antagonistic effects is not easy.

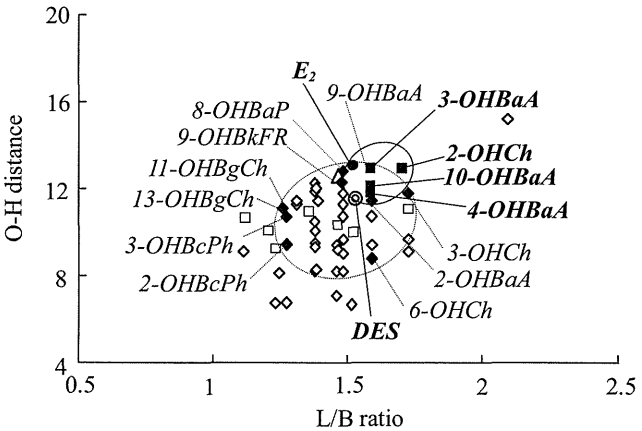

Fig. 2. Correlations between L/B ratio and O-H distance of estrogenic/antiestrogenic OHPAHs. hERα was used in the assay. ■: Relative effective potency of estrogenic activity (REP_E) > 0.001, □: REP_E < 0.001, ◆: Relative effective potency of antiestrogenic activity (REP_{AE}) > 0.1, ◇: REP_{AE} < 0.1, ◎: diethylstilbestrol (DES), ●: 17β-estradiol (E_2). In the case of E_2 and DES, O-O distance was used instead of O-H distance (Reproduced from ref. [25] with permission of Journal of Health Science).

Structural characteristic of oxidative stress induced by *ortho*-PAH quinones

The oxidative stress induced by PAHQs has been extensively studied and several reviews are available [33–37]. Among PAHQs, *ortho*-PAHQs could form either *ortho*-semiquinone anion radicals or catechols by electron nonenzymatic reduction. These compounds are unstable, and easily return to quinones. At that

time, superoxide anion radical and hydrogen peroxide are generated (Fig. 3). In addition, it was demonstrated that *ortho*-PAHQs, such as 9,10-phenanthrenequinone (9,10-PQ), can catalyze the transfer of electrons from dithiol to oxygen, generating superoxide anion radical. Regarding the *para*-quinone group, the generation of superoxide by semiquinone of Coenzyme Q (ubiquinone) has been also reported [38]. In fact, a large part of the electron leak to molecular oxygen results from the semiquinone form of CoQ generated during the Q-cycle in complex III or by a similar, less defined mechanism in complex I [39–41]. Therefore, most quinone compounds induce oxidative stress through an electronic mechanism induced by semiquinone.

We recently gathered more information about ROS generation from various PAHQs that exist in the atmosphere. In a study using thiol consumption as an index for ROS generation of PAHQs, we showed that *ortho*-PAHQs (9,10-PQ, 5,6-chrysenequinone (5,6-CQ) and benzo[*a*]pyrene-5,6-quinone (B[*a*]P-5,6-Q) consumed much more of the thiol groups, while *para*-PAHQs (1,4-naphthoquinone (1,4-NQ), 9,10-anthraquinone (9,10-AQ), 1,4-anthraquinone (1,4-AQ), 1,4-phenanthrenequinone (1,4-PQ), 1,2-benzoanthraquinone (1,2-BAQ), 1,4-chrysenequinone (1,4-CQ) and benzo[*c*]phenanthren-1,4-quinone (B[*c*]P-1,4-Q) didn't. We got the same results of viability for each PAHQ. Three of the *ortho*-PAHQs (9, 10-PQ, 5, 6-CQ and B[*c*]P-5,6-Q) significantly reduced the viability of A549 cells to about 20% of the control, but *para*-PAHQs had little effect on viability (Fig. 4). These results provided the initial evidence that there was a structure activity relationship by which *ortho*-PAHQs have a stronger potential for ROS generation than *para*-PAHQs.

Actually, several *ortho*-PAHQs such as 9,10-PQ and 9,10-AQ have been reported to exist in the atmosphere at the concentration range of 20 to 730 pg m^{-3} [18, 42, 43]. Other *ortho*-PAHQs with strong biological activities might also exist in the atmosphere. In addition, *ortho*-PAHQs can be generated in the human body through the metabolism of PAHs by cytochrome P4501A1 [44, 13]. Therefore, our data suggest that PAHQs, especially *ortho*-PAHQs, need to be paid more attention from the aspect of many kinds of diseases, such as pulmonary dysfunctional diseases, carcinogenesis, chronic inflammatory process, and acute symptomatic responses in the respiratory tract *et al.* [18, 45–47].

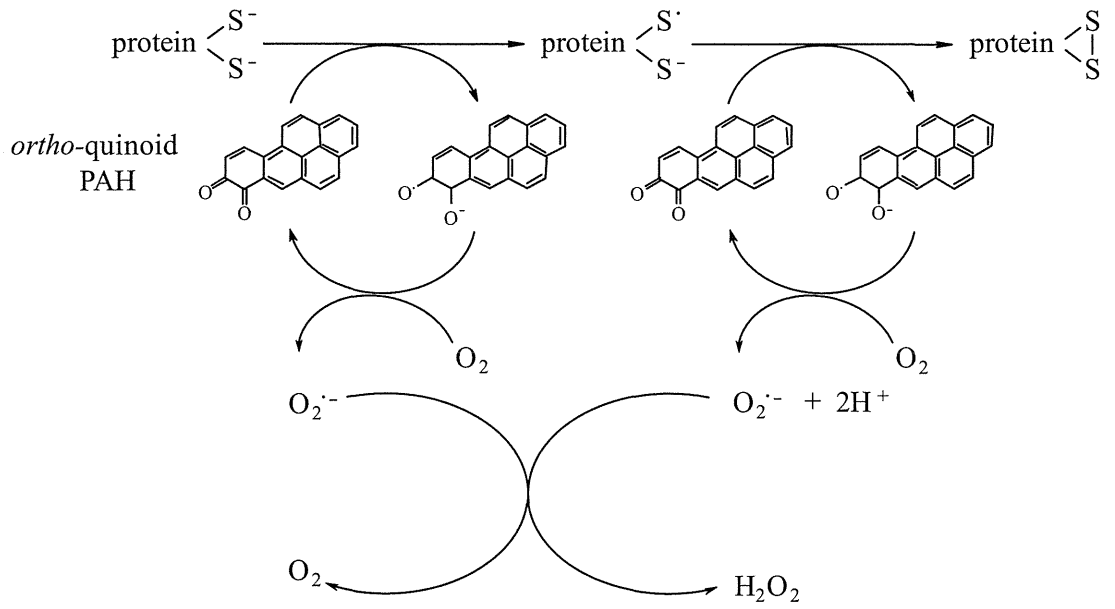

Fig. 3. Redox cycle for overproducing H_2O_2 by *ortho*-PAHQs.

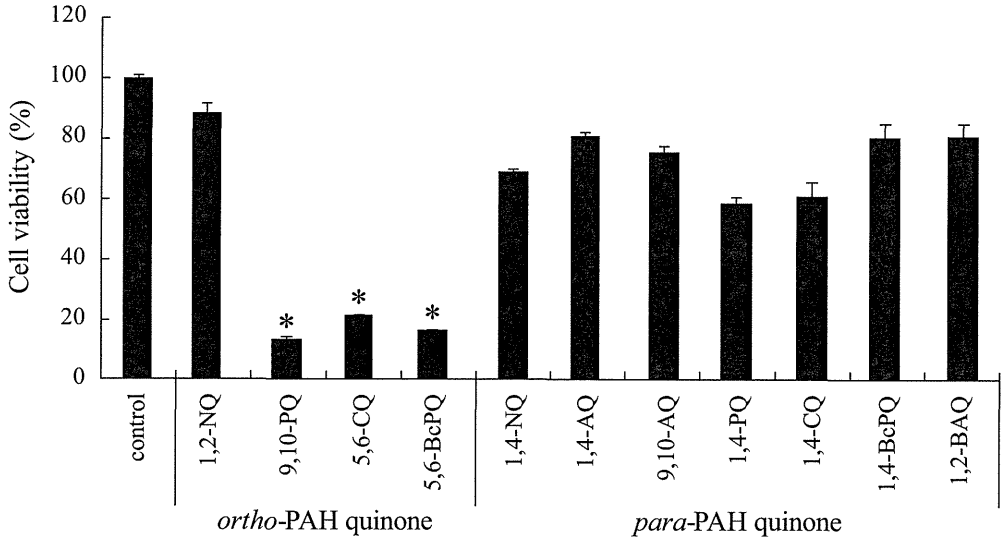

Fig. 4. Effects of PAHQs on the cell viability. A549 cells were incubated with 10 μM quinoid PAH for 12 h. The viability of the cells was determined by MTT assay. Each value is the mean ± SD of three determinations. Statistical significance, * : $P < 0.001$ vs. control (Reproduced from ref. [48] with permission of Journal of Health Science).

References

1. Ames BN, McCann J & Yamasaki E (1975): Methods for detecting carcinogens and mutagens with the salmonella/ mammalian-microsome mutagenicity test. Mutat Res 31: 347–364
2. IARC (1983): Chemical, Environmental and Experimental Data. Polynuclear Aromatic Compounds. Part 1, IARC Monographs 32: 1–477
3. IARC (2010): Some Non-heterocyclic Polycyclic Aromatic Hydrocarbons and Some Related Industrial Exposures. Air Pollution. Part 1, IARC Monographs 92: 1–868
4. Atkinson R & Arey J (1994): Atmospheric chemistry of gas-phase polycyclic aromatic hydrocarbons: formation of atmospheric mutagens. Environ Health Perspect 102: 117–126
5. Vione D, Barra S, Gennaro GDE, Rienzo MDE, Gilardoni S, Perrone MG & Pozzoli L (2004): Polycyclic aromatic hydrocarbons in the atmosphere: monitoring, sources, sinks and fate. II: Sinks and fate. Ann Chem 94: 17–32
6. Kameda T, Akiyama A, Toriba A, Tang N & Hayakawa K (2011): Atmospheric formation of hydroxynitropyrenes from a photochemical reaction of particle-associated 1-nitropyrene. Environ Sci Technol 45: 3325–3332
7. Nagy E, Zeisig M, Kawamura K, Hisamatsu Y, Sugeta A, Adachi S & Moller L (2005): DNA adduct and tumor formations in rats after intratracheal administration of the urban air pollutant 3-nitrobenzanthrone. Carcinogenesis 26: 1821–1828
8. Biswas S, Seema A & Rahman I (2006): Redox modifications of protein-thiols: emerging roles in cell signaling. Biochem Pharmacol 71: 551–564
9. Stadtman ER & Berlett BS (1997): Reactive oxygen-mediated protein oxidation in aging and disease. Chem Res Toxicol 10: 485–494
10. Valavanidis A, Vlahogianni T, Dassenakis M & Scoullos M (2006): Molecular biomarkers of oxidative stress in aquatic organisms in relation to toxic environmental pollutants. Ecotoxicol Environ Saf 64: 178–189
11. Stadtman ER & Levine RL (2003): Free radical-mediated oxidation of free amino acids and amino acid residues in proteins. Amino Acids 25: 207–218
12. Inoue K, Takano H, Hiyoshi K, Ichinose T, Sadakane K, Yanagisawa R, Tomura S & Kumagai Y (2007): Naphthoquinone enhances antigen-related airway inflammation in mice. Eur Respir J 29: 259–267

13. Xia T, Kovochich M & Nel A (2006): The role of reactive oxygen species and oxidative stress in mediating particulate matter injury. Clin Occup Environ Med 5: 817–836
14. Dellinger B, Prior WA, Cueto R, Squadrito GL, Hegde V & Deutsch WA (2001): Role of free radicals in the toxicity of airborne fine particulate matter. Chem Res Toxicol 14: 1371–1377
15. Pryor WA (1997): Cigarette smoke radicals and the role of free radicals in chemical carcinogenicity. Environ Health Perspect 105: 875–882
16. Oettinger R, Drumm K, Knorst M, Krinyak P, Smmolarski R & Kienast K (1999): Production of reactive oxygen intermediates by human macrophages exposed to soot particles and asbestos fibers and increase in NF- kappa B p50/p105 mRNA. Lung 177: 343–354
17. Sagai M, Lim HB & Ichinose T (2000): Lung carcinogenesis by diesel exhaust particles and the carcinogenic mechanism via active oxygens. Inhal Toxicol 12: 215–223
18. Cho AK, Stefano ED, You Y *et al* (2004): Determination of four quinones in diesel exhaust particles, SRM 1649a, and atmospheric PM2.5. Aerosol Sci Technol 38: 1–14
19. Hiyoshi K, Takano H, Inoue KI, Ichinose T, Yanagisawa R, Tomura S & Kumagai Y (2005b): Effects of phenanthraquinone on allergic airway inflammation in mice. Clin Exp Allergy 35: 1243–1248
20. Hiyoshi K, Takano H, Inoue K, Ichinose T, Yanagisawa R, Tomura S & Kumagai Y (2005a): Effects of a single intratracheal administration of phenanthraquinone on murine lung. J Appl Toxicol 25: 47–51
21. Meek MD (1998): Ah receptor and estrogen receptor-dependent modulation of gene expression by extracts of diesel exhaust particles. Environ Res 79: 114–121
22. Okamura K, Kizu R, Toriba A, Klinge CM & Hayakawa K (2002): Antiestrogenic activity of extracts of diesel exhaust particulate matter in MCF-7 human breast carcinoma cells. Polycyclic Aromatic Compd 22: 747–759
23. Taneda S, Hayashi H, Sakushima A, Seki K, Suzuki AK, Kamata K, Sakata M, Yoshino S, Sagai M & Mori Y (2002): Estrogenic and anti-estrogenic activities of two types of diesel exhaust particles. Toxicology 170: 153–161
24. Okamura K, Kizu R, Toriba A, Murahashi T, Mizokami A, Burnstein KL, Klinge CM & Hayakawa K (2004): Antiandrogenic activity of extracts of diesel exhaust particles emitted from diesel-engine truck under different engine loads and speeds. Toxicology 195: 243–54
25. Hayakawa K, Onoda Y, Tachikawa C, Hosoi S, Yoshida M, Chung SW, Kizu R, Toriba A, Kameda T & Tang N (2007): Estrogenic/antiestrogenic activities of polycyclic aromatic hydrocarbons and their monohydroxylated derivatives by yeast two-hybrid assay. J Health Sci 53: 562–570
26. Nishihara T, Nishikawa J, Kanayama T, Dakeyama F, Saito K, Imagawa M, Takatori S, Kitagawa Y, Hori S & Utsumi H (2000): Estrogenic activities of 517 chemicals by yeast two-hybrid assay. J Health Sci 46: 282–298
27. Hayakawa K, Bekki K, Yoshita M, Tachikawa C, Kameda T, Tang N, Toriba A & Hosoi S (2011): Estrogenic/antiestrogenic activities of quinoid polycyclic aromatic hydrocarbons. J Health Sci 57: 274–280
28. Hirose T, Morito K, Kizu R, Toriba A, Hayakawa K, Ogawa S, Inoue S, Muramatsu M & Masamune Y (2001): Estrogenic/antiestrogenic activities of benzo[*a*] pyrene monohydroxy derivatives. J Health Sci 47: 552–558
29. Hayakawa K, Onoda Y, Tachikawa C, Yoshita M, Toriba A, Kameda A & Tang N (2008): Interaction of hydroxylated polycyclic aromatic hydrocarbons to estrogen receptor. Polycycl Aromat Comp 28: 382–391
30. Hayakawa K, Bekki K, Yoshita M, Tachikawa C, Kameda T, Tang N, Toriba A & Hosoi S (2010): Estrogenic/antiestrogenic activities of quinoid polycyclic aromatic hydrocarbons. J Health Sci 57: 274–280
31. Fang H, Tong W, Shi LM *et al* (2001): Structure activity relationships for a large diverse set of natural, synthetic, and environmental estrogens. Chem Res Toxicol 14: 280–294
32. Tanenbaum DM, Wang Y, Williams SP & Sigler PB (1998): Crystallographic comparison of the estrogen and progesterone receptor's ligand binding domains. Proc Natl Acad Sci U.S.A 95: 5998–6003
33. O'Brien PJ (1991): Molecular mechanisms of quinone cytotoxicity. Chem Biol Interact 80: 1–41
34. Jarabal R, Harvey RG & Jarabak J (1998): Redox cycling of polycyclic aromatic hydrocarbon *o*-quinones: metal ion-catalyzed oxidation of catechols bypasses inhibition by superoxide dismutase. Chem Biol Interact

115: 201–213

35. Kumagai Y, Nakajima H, Midorikawa K, Homma-Takeda S & Shimojo N (1998): Inhibition of nitric oxide formation by neuronal nitric oxide synthase by quinones: Nitric oxide synthase as a quinones reductase. Chem Res Toxicol 11: 608–613
36. Penning TM, Butczynski ME, Hung CF, McCoull KD, Palackal NT & Tsuruda LS (1999): Dihydrodiol dehydrogenases and polycyclic aromatic hydrocarbon activation: Generation of reactive and redox active o-quinones. Chem Res Toxicol 12: 1–12
37. Kumagai Y, Koide S, Taguchi K, Endo A, Nakai Y, Yoshikawa T & Shimojo N (2000): Oxidation of proximal protein sulfhydryls by phenanthrenequinone, a component of diesel exhaust particles. Chem Res Toxicol 15: 483–489
38. Herlein JA, Fink BD, Henry DM, Yorek MA, Teesch LM & Sivitz WI (2011): Mitochondrial superoxide and coenzyme Q in insulin-deficient rats: increased electron leak. Am J Physiol Requl Inteqr Comp Physiol 301: 1616–1624
39. Brandt U (2006): Energy-converting NADH: Quinone oxidoreductase (complex I). Annu Rev Biochem 75: 69–92
40. Dutton PL, Moser CC, Sled VD, Daldal F & Ohnishi T (1998): A reductant-induced oxidation mechanism for complex I. Biochim Biophys Acta 1364: 245–257
41. Lambert AJ & Brand MD (2004): Inhibitors of the quinone-binding site allow rapid superoxide production from mitochondrial NADH: Ubiquinone oxidoreductase (complex I). J Biol Chem 279: 39414–39420
42. Bolton J, Trush MA, Penning TM, Dryhurst G & Monks TJ (2000): Role of quinones in toxicology. Chem Res Toxicol 13: 135–160
43. Chung SW (2007): Studies of environmental quinoid PAHs on their potential human adverse health effects in priority oxidative stress. Doctor thesis, Kanazawa University: 1–98
44. Lintelmann J, Fischer K, Karg E & Schrppel A (2005): Determination of selected polycyclic aromatic hydrocarbons and oxygenated polycyclic aromatic hydrocarbons in aerosol samples by high performance liquid chromatography and liquid chromatography-tandem mass spectrometry. Anal Bioanal Chem 381: 508–519
45. Turuda L, Hou YT & Penning TM (2001): Stable expression of rat dihydrodiol dehydrogenase (AKR1C9) in human breast MCF-7 cells results in the function of PAH-*o*-quinones and enzyme mediated cell death. Chem Res Toxicol 14: 856–862
46. Tao F, Gonzalez-Flecha B & Kobzik L (2003): Reactive oxygen species in pulmonary inflammation by ambient particulates. Free Radic Biol Med 35: 327–340
47. Lin PH, Pan WC, Kang YW, Chen YL, Lin CH, Lee MC, Chou YH & Nakamura J (2005): Effects of naphthalene quinoids on the induction of oxidative DNA and in human cultured cells. Chem Res Toxicol 18: 1262–1270
48. Motoyama Y, Bekki K, Chung S-W, Tang N, Kameda T, Toriba A, Taguchi K & Hayakawa K (2009): Oxidative stress more strongly induced by *ortho*- than *para*-quinoid polycyclic aromatic hydrocarbons in A549 cells. J Health Sci 55: 845–850

多環芳香族炭化水素誘導体が示す毒性作用

戸次　加奈江[1]，鳥羽　陽[2]，唐　寧[2,3]，亀田　貴之[2]，早川　和一[2]

[1]金沢大学大学院　自然科学研究科　環境科学専攻
[2]金沢大学　医薬保健領域薬学系
[3]兵庫医科大学　公衆衛生学

要　　旨：多環芳香族炭化水素類(PAHs)は大気粉塵などの多種類の環境汚染物質に含まれ，長年の研究によって多様な生体影響を引き起こすことが知られている．一方で，PAHsは生体内での代謝反応や，大気中での化学反応によって多種多様な誘導体を生成することが知られている．近年では，PAHだけでなくPAH誘導体の毒性影響が着目されており，エストロゲン様/抗エストロゲン作用，酸化ストレス反応など，PAHとは異なる誘導体独自の毒性影響の存在が報告されている．また，生成するPAH誘導体には多くの構造異性体が存在するが，PAH誘導体が示す毒性作用と構造との間に相関性，いわゆる構造活性相関があることが示されている．以上の研究は，環境中に存在するPAH誘導体の生体影響を解明する上で重要な研究であるとともに，多種多様なPAH誘導体の総合的な毒性影響予測に貢献できると考えられる．

キーワード：PAH誘導体，構造活性相関，エストロゲン様/抗エストロゲン作用，活性酸素種．

J UOEH(産業医大誌)35(1)：17－24(2013)

ZOOLOGICAL SCIENCE 30: 217–223 (2013)

Static and Dynamic Hypergravity Responses of Osteoblasts and Osteoclasts in Medaka Scales

Sachiko Yano[1,2], Kei-ichiro Kitamura[3], Yusuke Satoh[3], Masaki Nakano[4], Atsuhiko Hattori[4], Toshio Sekiguchi[2], Mika Ikegame[5], Hiroshi Nakashima[3], Katsunori Omori[6], Kazuichi Hayakawa[7], Atsuhiko Chiba[8], Yuichi Sasayama[2], Sadakazu Ejiri[9], Yuko Mikuni-Takagaki[10], Hiroyuki Mishima[11], Hisayuki Funahashi[12], Tatsuya Sakamoto[13], and Nobuo Suzuki[2]*

[1]*Japan Aerospace Exploration Agency, Tsukuba, Ibaraki 305-8505, Japan*
[2]*Noto Marine Laboratory, Institute of Nature and Environmental Technology, Kanazawa University, Housu-gun, Ishikawa 927-0553, Japan*
[3]*Institute of Health Sciences, College of Medical, Pharmaceutical and Health Sciences, Kanazawa University, Kanazawa, Ishikawa 920-0942, Japan*
[4]*Department of Biology, College of Liberal Arts and Sciences, Tokyo Medical and Dental University, Ichikawa, Chiba 272-0827, Japan*
[5]*Department of Oral Morphology, Graduate School of Medicine, Dentistry and Pharmaceutical Sciences, Okayama University, Okayama, Okayama 700-8525, Japan*
[6]*Faculty of Economics, Asia University, Musashino, Tokyo 180-8629, Japan*
[7]*Institute of Pharmaceutical Sciences, College of Medical, Pharmaceutical and Health Sciences, Kanazawa University, Kanazawa, Ishikawa 920-1192, Japan*
[8]*Department of Materials and Life Sciences, Sophia University, Tokyo 102-8554, Japan*
[9]*Department of Oral Anatomy, Division of Oral Structure, Function and Development, Asahi University School of Dentistry, Hozumi, Gifu 501-0296, Japan*
[10]*Department of Functional Biology, Kanagawa Dental College, Yokosuka, Kanagawa 238-8580, Japan*
[11]*Department of Human Life Sciences, Kochi Gakuen College, Kochi 780-0955, Japan*
[12]*Department of Anatomy, Showa University School of Medicine, Shinagawa-ku, Tokyo 142-8555, Japan*
[13]*Ushimado Marine Institute, Okayama University, Ushimado, Okayama 701-4303, Japan*

Fish scales are a form of calcified tissue similar to that found in human bone. In medaka scales, we detected both osteoblasts and osteoclasts and subsequently developed a new scale assay system. Using this system, we analyzed the osteoblastic and osteoclastic responses under 2-, 3-, and 4-gravity (G) loading by both centrifugation and vibration. After loading for 10 min, the scales from centrifugal and vibration loading were incubated for 6 and 24 hrs, respectively, after which the osteoblastic and osteoclastic activities were measured. Osteoblastic activity significantly increased under 2- to 4-G loading by both centrifugation and vibration. In contrast, we found that osteoclastic activity significantly decreased under 2- and 3-G loading in response to both centrifugation and vibration. Under 4-G loading, osteoclastic activity also decreased on centrifugation, but significantly increased under 4-G loading by vibration, concomitant with markedly increased osteoblastic activity. Expression of the receptor activator of the NF-κB ligand (RANKL), an activation factor of osteoclasts expressed in osteoblasts, increased significantly under 4-G loading by vibration but was unchanged by centrifugal loading. A protein sequence similar to osteoprotegerin (OPG), which is known as an osteoclastogenesis inhibitory factor, was found in medaka using our sequence analysis. The ratio of RANKL/OPG-like mRNAs in the vibration-loaded scales was significantly higher than that in the control scales, although there was no difference between centrifugal loaded scales and the control scales. Accordingly, medaka scales provide a useful model by which to analyze bone metabolism in response to physical strain.

Key words: osteoblast, osteoclast, scale, medaka, gravity response, RANKL, OPG

INTRODUCTION

Various in vitro models have been developed elucidate the effect of physical strain, including the response of bone metabolism to different gravitational loads, (Tjandrawinata et al., 1997; Tanaka et al., 2003; Peng et al., 2011). Most studies using in vitro models noted osteoblastic responses to physical strain as the determinant in bone (Tjandrawinata et al., 1997; Tanaka et al., 2003). Bone consists of osteoblasts, osteoclasts, and the bone matrix, and both cell-to-cell and cell-to-matrix interactions are critical for cell response to physical stress (Harter et al., 1995; Owan et al., 1997; Hoffler et al., 2006). It was recently reported that mechanical

* Corresponding author. Tel. : +81-768-74-1151;
Fax : +81-768-74-1644;
E-mail: nobuos@staff.kanazawa-u.ac.jp
doi:10.2108/zsj.30.217

stretch-induced calcium efflux from bone matrix and stimulated osteoblasts, suggesting that the bone matrix acts as a reservoir for mechanochemical transducers, which convert mechanical strain into a chemical signal for the onset of calcium efflux (Sun et al., 2012). A co-culture system of osteoblasts and osteoclasts with the matrix is essential to elucidate bone metabolism under gravity (G) loading conditions, indicating the need for the development of such a system.

The teleost scale, a calcified tissue, contains osteoblasts and osteoclasts (Bereiter-Hahn and Zylberberg, 1993, Suzuki et al., 2000; Yoshikubo et al., 2005) that are similar to those found in avian and mammalian membrane bone. Moreover, multinucleated osteoclasts, an active type of osteoclast, have been detected by tartrate-resistant acid phosphatase (TRAP) staining in the scales of goldfish (Suzuki et al., 2000; Azuma et al., 2007; Suzuki et al., 2011), carp (de Vrieze et al., 2010), and rainbow trout (Persson et al., 1999), together with the osteoblasts detected by alkaline phosphatase (ALP) staining (de Vrieze et al., 2010). With such typical components of bone matrix as type I collagen (Zylberberg et al., 1992), bone γ-carboxyglutamic acid protein (Nishimoto et al., 1992), osteonectine (Lehane et al., 1999), and hydroxyapatite (Onozato and Watabe, 1979), a teleost scale is a suitable model for mammalian bone.

Medaka (*Oryzias latipes*), a small teleost, is a particularly suitable model organism, as its entire genome sequence has been mapped, facilitating genetic analysis. Its relatively short life cycle and high productivity (Kasahara et al., 2007; Kawakami, 2007; Takeda, 2008) are also valuable features. Therefore, medaka appears to be a model organism that can be used to analyze various biological processes, including bone metabolism, at the molecular level (Inohaya et al., 2007; Watanabe-Asaka et al., 2010). Medaka were launched into space in 1994 as part of a microgravity experiment (Ijiri, 1995). This experiment included the first observation of the mating behavior, development, and hatching of a vertebrate in space. Using medaka, we can analyze the response of osteoblasts and osteoclasts, not only in a hypergravity environment on the ground but also under microgravity conditions in space.

In the present study, we investigated bone metabolism under G-loading using medaka scales as a bone model. To demonstrate the coexistence of bone cells in medaka scales, we first analyzed the morphological features of both osteoblasts and osteoclasts. Second, we developed a new in vitro assay system using medaka scales. In this system, ALP and TRAP were used as respective markers of osteoblasts and osteoclasts. Third, we examined static (centrifugation) and dynamic (vibration) G-loading using the developed assay system with medaka scales. We demonstrated that osteoblasts and osteoclasts in medaka scales responded with certain degrees of sensitivity to G-loading by both centrifugation and vibration. Using our original system with medaka scales, we measured the difference between static and dynamic G-loading.

MATERIALS AND METHODS

Animals

Medaka were purchased from a commercial source (Higashikawa Fish Farm, Yamatokoriyama, Japan) and used for the in vitro scale assay. All experimental procedures were conducted in accordance with the Guidelines for the Care and Use of Laboratory Animals of Kanazawa University, Japan.

Morphological study of osteoblasts and osteoclasts in medaka scales

Scales were collected from medaka anesthetized with ethyl 3-aminobenzoate, methanesulfonic acid salt (Sigma-Aldrich, Inc., St. Louis, MO, USA) and fixed using 4% paraformaldehyde solution neutralized with phosphate buffer solution (pH 7.2; Wako, Co., Ltd., Osaka, Japan). Subsequently, osteoblasts were detected by ALP staining using NBT/BCIP Stock Solution (Roche Applied Science, Mannheim, Germany). The scales were TRAP stained using the methods described by Cole and Walters (1987). After staining, the osteoblasts and osteoclasts were observed under a microscope.

Development of an in vitro assay system using medaka scales

Medaka were anesthetized with ethyl 3-aminobenzoate, methanesulfonic acid salt (Sigma-Aldrich, Inc., St. Louis, MO, USA), after which all scales collected from the left side of the animal were placed into a 1.5-mL microtube and all scales collected from the right side of medaka were transferred into a different 1.5-mL microtube. One hundred microliters of distilled water were added to each microtube. After sonication, the tube was centrifuged and the supernatant was used to detect both ALP and TRAP activities. The methods for measuring ALP and TRAP activities were reported by Suzuki et al. (2007). The ALP and TRAP data obtained for the scales from the left and right sides of the medaka were compared.

Effect of osteoblastic and osteoclastic activities under 2-, 3-, and 4-G loading by centrifugation and vibration

Scales were collected from medaka anesthetized with ethyl 3-aminobenzoate, methanesulfonic acid salt. All the left-side scales (loaded experimental scales) and right-side scales (unloaded control scales) from each individual were put into respective microtubes, followed by the addition of a 500-μL aliquot of Leibovitz's L-15 medium (Invitrogen, Grand Island, NY, USA) containing a 1% penicillin–streptomycin mixture (ICN Biomedicals, Inc., Aurora, OH, USA). To fix the scales, a cotton ball (1 cm in diameter) was placed into each microtube. The microtube containing the scales was loaded to 2-, 3-, and 4-G by centrifugation (LIX-130; Tomy Digital Biology Co., Ltd., Tokyo, Japan) or by vibration with the original apparatus (Suzuki et al., 2007) for 10 min at room temperature. The loaded scales were compared with unloaded (1-G control) scales. The loading times were determined following our previous study using goldfish scales (Suzuki et al., 2007). After loading, the centrifuged and vibrated scales were incubated for 6 and 24 hrs, respectively, at 15°C. We previously reported that calcemic hormones such as calcitonin and estrogen were effective at these incubation times (Suzuki et al., 2000; Yoshikubo et al., 2005); therefore, we used these times in the present study. After incubation, the ALP and TRAP activities in the medaka scales were measured as described above.

Analysis of the interaction between osteoblasts and osteoclasts under 4-G loading by centrifugation and vibration

We analyzed the mRNA expression of both the receptor activator of the NF-κB ligand (RANKL), an activating factor of osteoclasts expressed in osteoblasts, and osteoprotegerin (OPG), an osteoclastogenesis inhibitory factor in osteoblasts. OPG, a decoy receptor of RANKL, inhibits osteoclastogenesis by binding to RANKL (see the review by Lacey et al., 2012). To analyze the interaction between osteoblasts and osteoclasts, the ratio of the expression of the RANKL/OPG-like mRNA was examined.

After 4-G loading, the scales were incubated for 24 hrs at 15°C and then frozen at −80°C for mRNA analysis. The loaded scales were compared with unloaded (1-G control) scales. Total RNAs

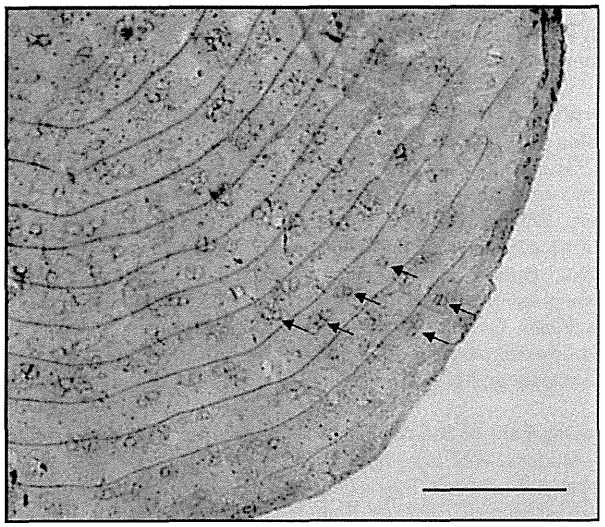

Fig. 1. Microscopic views of medaka scales stained for alkaline phosphatase (ALP). Arrows indicate ALP positive cells. Bar: 100 μm.

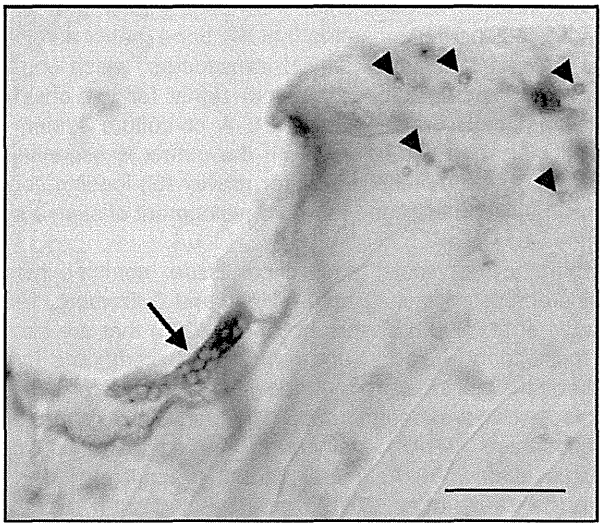

Fig. 2. Microscopic views of medaka scales stained for tartrate-resistant acid phosphatase. Arrowheads and arrows indicate mono- and multi-nucleated osteoclastic cells, respectively. Bar: 100 μm.

were prepared from medaka scales using a total RNA isolation kit for fibrous tissue (Qiagen GmbH, Hilden, Germany). Complementary DNA was synthesized using the PrimeScript™ RT reagent kit (Takara Bio Inc., Otsu, Japan). The primer sequences—sense: AGGCAAAACGGCAAAGAAAT; anti-sense: CCCAGCTTTATGGCTCCAA—were designed from medaka RANKL (JN119285) (To et al., 2012). The OPG-like sequence in medaka was determined by sequence analysis, as follows. All amino acid sequences of medaka were retrieved from the Genome to Protein Structure and Function database. We analyzed the amino acid sequence of OPG in fugu (ENSTRUP00000023772) as a query to all amino acid sequences of medaka, and selected the best-hit sequence as the candidate for the OPG amino acid sequence of medaka. Thereafter, we used CLUSTAL X2 (Larkin et al., 2007) for multiple sequence alignment of homologous sequences. The primers for the OPG-like sequence in medaka were as follows: sense: 5′-GGATCCGTCCACTGGTAAAA-3′; antisense: 5′-GAGCACTCGATTTCCACCTC-3′.

β-actin (ENSORLT00000021168) was amplified using the following primers: sense: 5′-TGTGCTACGTGGCTCTTGAC-3′; antisense: 5′-GCCAATGAAAGAAGGTTGGA-3′. The PCR amplification was performed using the real-time Mx3000p PCR apparatus (Agilent Technologies, Santa Clara, CA, USA) (Suzuki et al., 2011). The annealing temperature of RANKL, OPG-like, and β-actin fragments was 60°C. The initial reaction condition was 10 s at 95°C, followed by 40 cycles of denaturation at 95°C for 5 s, and annealing/extension at 60°C for 40 s. The RANKL and OPG-like mRNA levels were normalized to the β-actin mRNA level.

Statistical analysis

All results are expressed as means ± SEM (n = 10). The data were assessed using the paired t-test and the significance level chosen was $P < 0.05$.

RESULTS

Osteoblasts and osteoclasts in medaka scales

In the medaka scales, ALP-stained osteoblasts (Fig. 1) and TRAP-stained mono- and multi-nucleated osteoclastic cells were detected (Fig. 2).

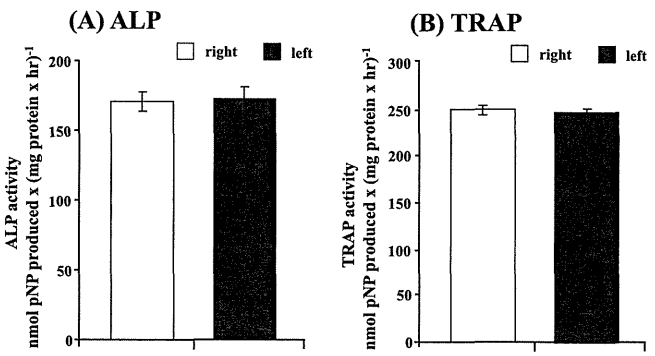

Fig. 3. Comparison of osteoblastic **(A)** and osteoclastic **(B)** activity in medaka scales from the right and left sides of the medaka body.

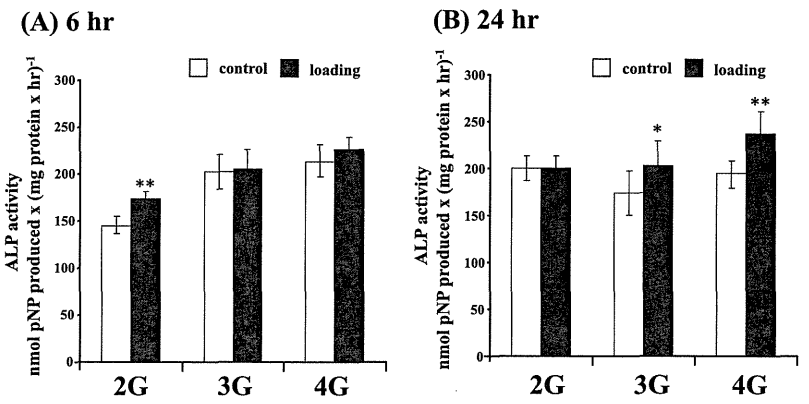

Fig. 4. Effect of osteoblastic activity after incubation for 6 **(A)** and 24 hrs **(B)** under 2-gravity (G), 3-G, 4-G loading by centrifugation. * and ** indicate statistically significant differences at $P < 0.05$ and $P < 0.01$, respectively, from the values in the control scales.

Comparison of ALP and TRAP activities between scales from the left and right sides of medaka

ALP activity in scales from the left side of medaka was similar to that in scales from the right side (Fig. 3A) with no significant difference. The TRAP activity in the scales from the left side was nearly equal to that in scales from the right side (Fig. 3B).

Effect of osteoblastic and osteoclastic activities under 2-, 3-, and 4-G loading by centrifugation

The ALP activity significantly increased under 2-G loading by centrifugation after 6 hrs of incubation (Fig. 4A). The ALP activity increased significantly under 3- and 4-G loading by centrifugation after 24 hrs of incubation (Fig. 4B). In contrast, under 2- to 4-G loading by centrifugation, the TRAP activity significantly decreased after both 6 and 24 hrs of incubation (Fig. 5A, B).

Effect of osteoclastic and osteoblastic activity under 2-, 3-, 4-G loading by vibration

The ALP activity increased significantly under 3- and 4-G loading by vibration after 6 hrs of incubation (Fig. 6A). Under 2- to 4-G loading by vibration, the ALP activity significantly increased after 24 hrs of incubation (Fig. 6B). Under 3-G loading by vibration, the TRAP activity significantly decreased after 6 hrs of incubation (Fig. 7A). After 24 hrs of incubation, the TRAP activity significantly decreased under 2-G loading but significantly increased under 4-G loading by vibration (Fig. 7B).

Determination of the OPG-like sequence in medaka

Using our original system, the OPG-like sequence was determined from the medaka database. After analysis using CLUSTAL X2, we found that 18 cysteines are strictly conserved in fish, birds, and mammals (Fig. 8). The amino acid identity of the medaka OPG-like sequence was 69.9% compared to the fugu OPG, 38.3% compared to the chicken OPG, 39.0% compared to the mouse OPG, and 41.2% compared to the human OPG. Furthermore, similarity analysis using the BLOSUM62 matrix confirmed that the medaka OPG-like sequence shows a high similarity to fugu (80.1%) and a relatively high similarity to other vertebrate OPG (chicken, 60.0%; mouse, 58.0%; human, 58.3%).

Analysis of the interaction between osteoblasts and osteoclasts under 4-G loading by centrifugation and vibration

RANKL mRNA expression was increased significantly by vibration loading, but not by

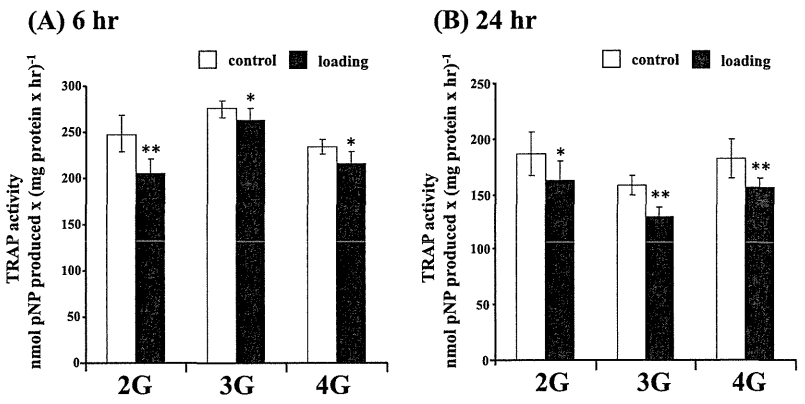

Fig. 5. Effect of osteoclastic activity after incubation for 6 **(A)** and 24 hrs **(B)** under 2-gravity (G), 3-G, 4-G loading by centrifugation. * and ** indicate statistically significant differences at $P < 0.05$ and $P < 0.01$, respectively, from the values in the control scales.

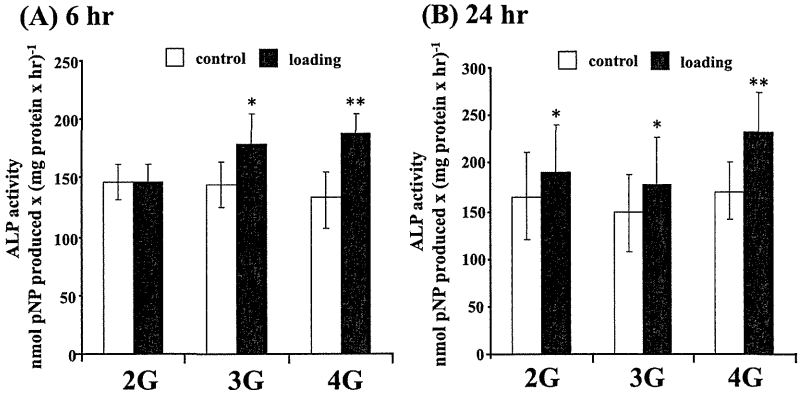

Fig. 6. Effect of osteoblastic activity after incubation for 6 **(A)** and 24 hrs **(B)** under 2-gravity (G), 3-G, 4-G loading by vibration. * and ** indicate statistically significant differences at $P < 0.05$ and $P < 0.01$, respectively, from the values in the control scales.

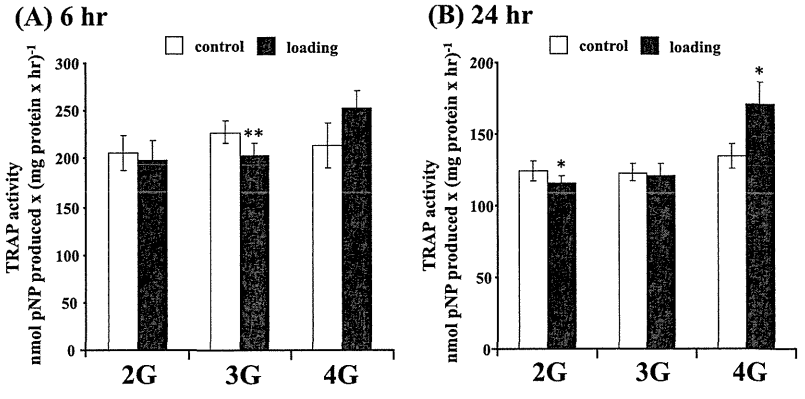

Fig. 7. Effect of osteoclastic activity after incubation for 6 **(A)** and 24 hrs **(B)** under 2-gravity (G), 3-G, 4-G loading by vibration. * and ** indicate statistically significant differences at $P < 0.05$ and $P < 0.01$, respectively, from the values in the control scales.

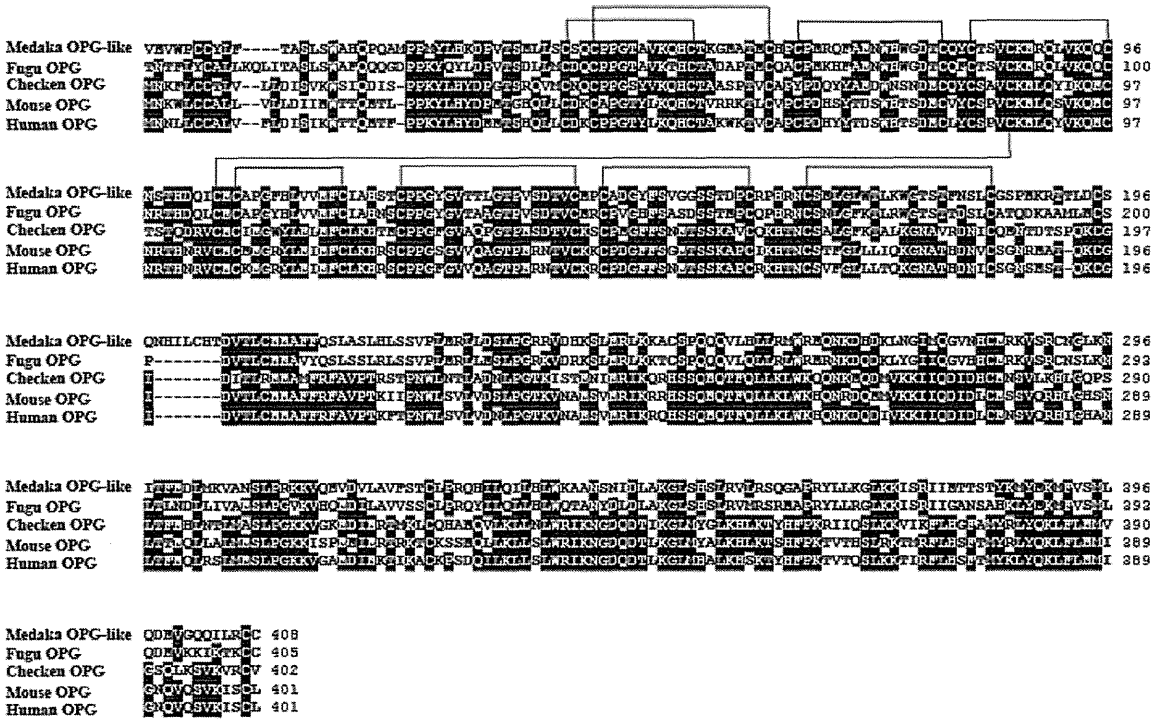

Fig. 8. Multiple protein sequence alignment of osteoprotegerin (OPG) with other animals: fugu OPG (ENSTRUP00000023772), chicken OPG (ENSGALP00000025915), mouse OPG (PRO_0000034588), and human OPG (PRO_0000034587), and concatenated cysteines represent disulfide bonds in OPG sequences. This multiple protein sequence alignment showed that disulfide bonds are highly conserved in the OPG sequences of vertebrates.

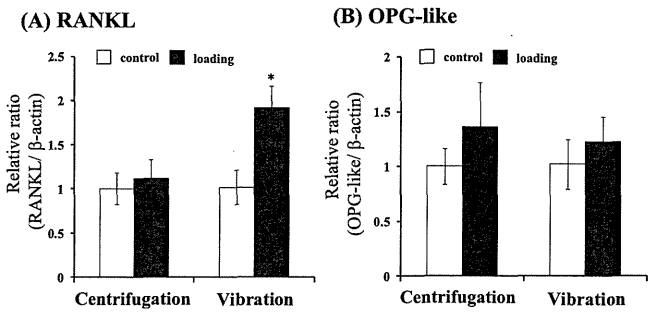

Fig. 9. Changes in expression of the receptor activator of NF-κB ligand (RANKL) **(A)** and osteoprotegerin- (OPG-) like mRNA **(B)** under 4-gravity loading by centrifugation and vibration. * indicates statistically significant difference at $P < 0.05$ from the values in the control scales.

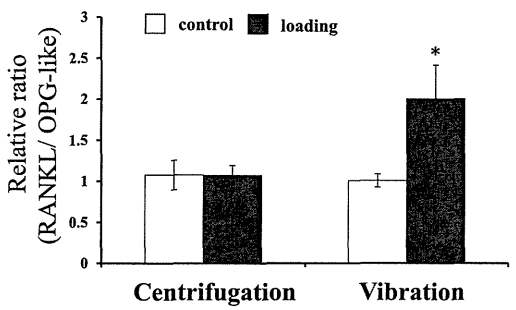

Fig. 10. The ratio of expression of RANKL/OPG-like mRNA in the centrifugal- and vibration-loaded scales. * indicates statistically significant difference at $P < 0.05$ from the values in the control scales.

centrifugal loading (Fig. 9A). The expression of the OPG-like mRNA was not significantly different between centrifugal and vibration loading (4-G) (Fig. 9B). The ratio of the expression of RANKL/OPG-like mRNA in the vibration-loaded scales was significantly higher than that in the control scales (Fig. 10).

DISCUSSION

The present study is the first to demonstrate that medaka scales respond to G-loading by using ALP and TRAP as marker enzymes of osteoblasts and osteoclasts stained by the respective substrates (Figs. 1, 2), supporting the notion that this new assay system can be a useful tool in analyzing the response of these cells to gravitational stress.

Osteoblasts in medaka scales were activated by loading with increasing gravity (2-G, 3-G, and 4-G) for 10 min by centrifugation. Medaka scales responded to G-force < 5, which is much lower than the 5 to 50 G needed for mammalian osteoblasts to respond (Gebken et al., 1999; Saito et al., 2003; Searby et al., 2005), suggesting that medaka scales are very sensitive to G-loading. In addition, the osteoclastic activity in medaka scales decreased under 2-G, 3-G, and 4-G loading by centrifugation, suggesting a very good response of osteoclasts to low G loading, although the mechanisms have yet to be determined. Moreover, osteoblastic and osteoclastic activities in medaka scales were sensitive not only to dynamic G-loading by vibration with a G-load apparatus, but also to static G-loading by centrifugation. Fish scales contain osteoblasts, osteoclasts, and a matrix similar to that in bone (Bereiter-Hahn and Zylberberg,

1993; Suzuki et al., 2000; Yoshikubo et al., 2005; Azuma et al., 2007). Bone matrix plays an important role in the response to physical stress (Owan et al., 1997; Hoffer et al., 2006); in future studies, we will seek to identify the difference in matrix components, if any, to elucidate the mechanisms underlying the extreme sensitively of medaka scales to G-loading.

The interaction between osteoblasts and osteoclasts has been reported in mammals, and cytokine from osteoblasts, in particular, is required to produce differentiated osteoclasts (Suda et al., 1999). RANK in osteoclasts binds RANKL, the ligand, resulting in osteoclast activation whereby multinucleated osteoclasts (an active type of osteoclast) are formed (Teitelbaum et al., 2000). OPG, a decoy receptor of RANKL, inhibits osteoclastogenesis by binding to RANKL (see the review by Lacey et al., 2012). We demonstrated that RANKL mRNA expression increases significantly in response to vibration loading, but not centrifugal loading. In addition, the ratio of the expression of RANKL/OPG-like mRNA in the scales loaded by vibration was significantly higher than that in control scales, while there was no difference on centrifugation. Because the RANKL/OPG ratio is an indicator of bone resorption (Lacey et al., 2012), medaka scales provide a good model by which to investigate bone metabolism.

In a study of a widely used hind-limb-elevation (tail suspension) model, the results of bone resorption by osteoclasts were inconsistent (Carmeliet et al., 2001); in this field, most subsequent research has thus been focused on osteoblastic response in bone formation. Recently, in isolated osteoclasts, it was reported that osteoclastic activity increased in those osteoclasts that were cultured in space (Tamma et al., 2009); however, there has been no data relating the interaction between osteoblasts and osteoclasts in space. Although bone mass is reportedly increased by mechanical strain, it has also been reported that mechanical strain on isolated osteoclasts upregulated their bone-resorbing activity (Kurata et al., 2001); therefore, the results obtained from the isolated osteoclast system may differ from that obtained from the in vivo system. Moreover, we demonstrated that melatonin, a major hormone secreted from the pineal gland, activated the growth of isolated osteoblasts in culture, although this hormone also suppressed the functions of osteoblasts using an in vitro assay system with scales (Suzuki and Hattori, 2002). These results obtained using an in vitro assay system resembled those of an in vivo study in rats (Ladizesky et al., 2003). Based on these results, we propose that our study using a scale-organ-culture system provides more accurate reproduction of the in vivo study.

Medaka has a number of beneficial features as a model organism, and transgenic systems have been developed using this species. For example, fluorescent protein markers of osteoblasts can be observed in vivo (Inohaya et al., 2007). Furthermore, the launch of the aquatic animal habitation module (Aquatic Habitat), which is planned for the near future, will enable breeding medaka in the International Space Station (Sakimura et al., 2003; Watanabe-Asaka et al., 2010). We will be able to perform space experiments using the scales of space-bred medaka, both in vitro and in vivo, in the near future. Together with the present data, medaka scales provide a promising model system by which to study bone metabolism, and will also be useful in evaluating the physical strain associated with gravity and microgravity in space flight.

ACKNOWLEDGMENTS

This study was supported in part by grants to N.S. (Kurita Water and Environment Foundation; Grant-in-Aid for Space Utilization by the Japan Aerospace Exploration Agency; Grant-in-Aid for Scientific Research [C] Nos. 21500404 and 24620004 by JSPS), to A.H. (Grant-in-Aid for Scientific Research [C] Nos. 21570062 and 24570068 by JSPS), to K.K. (Grant-in-Aid for Scientific Research [C] Nos. 21500681 and 24500848 by JSPS), to T.S. (Grant-in-Aid for Young Scientists [B] Nos. 22770069 and 40378568 by JSPS), to H.M. (Grant-in-Aid for Scientific Research [C] No. 23592727 by JSPS), and to K.H. (the Environment Research and Technology Development Fund [B-0905] sponsored by the Ministry of the Environment, Japan; Health, Labour Sciences Research Grants of the Ministry of Health, Labour and Welfare, Japan; Grant-in-Aid for Scientific Research [B] No. 21390034 and for Exploratory Research No. 24651044 by JSPS).

REFERENCES

Azuma K, Kobayashi M, Nakamura M, Suzuki N, Yashima S, Iwamuro S, et al. (2007) Two osteoclastic markers expressed in multinucleate osteoclasts of goldfish scales. Biochem Biophys Res Commun 362: 594–600

Bereiter-Hahn J, Zylberberg L (1993) Regeneration of teleost fish scale. Comp Biochem Physiol 105A: 625–641

Carmeliet G, Vico L, Bouillon R (2001) Space flight: A challenge for normal bone homeostasis. Crit Rev Eukaryot Gene Expr 11: 131–144

Cole AA, Walters LM (1987) Tartrate-resistant acid phosphatase in bone and cartilage following decalcification and cold-embedding in plastic. J Histochem Cytochem 35: 203–206

de Vrieze E, Mets JR, Von den Hoff JW, Flik G (2010) ALP, TRAcP and cathepsin K in elasmoid scales: A role in mineral metabolism. J Appl Ichthyol 26: 210–213

Gebken J, Lüders B, Notbohm H, Klein HH, Brinckmann J, Müller PK, Bätge B (1999) Hypergravity stimulates collagen synthesis in human osteoblast-like cells: Evidence for the involvement of p44/42 MAP-kinases (ERK 1/2). J Biochem 126: 676–682

Harter LV, Hruska KA, Duncan RL (1995) Human osteoblast-like cells respond to mechanical strain with increased bone matrix protein production independent of hormonal regulation. Endocrinology 136: 528–535

Hoffler CE, Hankenson KD, Miller JD, Bilkhu SK, Goldstein SA (2006) Novel explant model to study mechanotransduction and cell-cell communication. J Orthop Res 24: 1687–1698

Ijiri K (1995) Fish mating experiment in space - What it aimed at and how it was prepared. Biol Sci Space 9: 3–16

Inohaya K, Takano Y, Kudo A (2007) The teleost intervertebral region acts as a growth center of the centrum: *In vivo* visualization of osteoblasts and their progenitors in transgenic fish. Dev Dyn 236: 3031–3046

Kasahara M, Naruse K, Sasaki S, Nakatani Y, Qu W, Ahsan B, et al. (2007) The medaka draft genome and insights into vertebrate genome evolution. Nature 447: 714–719

Kawakami K (2007) Tol2: A versatile gene transfer vector in vertebrates. Genome Biol 8 Suppl 1: S7.1–S7.10

Kurata K, Uemura T, Nemoto A, Tateishi T, Murakami T, Higaki H, et al. (2001) Mechanical strain effect on bone-resorbing activity and messenger RNA expressions of marker enzymes in isolated osteoclast culture. J Bone Miner Res 16: 722–730

Lacey DL, Boyle WJ, Simonet WS, Kostenuik PJ, Dougall WC, Sullivan JK, et al. (2012) Bench to bedside: Elucidation of the

OPG-RANK-RANKL pathway and the development of denosumab. Nat Rev Drug Discov 11: 401–419
Ladizesky MG, Boggio V, Albornoz LE, Castrillón PO, Mautalen C, Cardinali DP (2003) Melatonin increases oestradiol-induced bone formation in ovariectomized rats. J Pineal Res 34: 143–151
Larkin MA, Blackshields G, Brown NP, Chenna R, McGettigan PA, McWilliam H, et al. (2007) Clustal W and Clustal X version 2.0. Bioinformatics 23: 2947–2948
Lehane DB, Mckie N, Russell RGG, Henderson IW (1999) Cloning of a fragment of the osteonection gene from goldfish, *Carassius auratus*: Its expression and potential regulation by estrogen. Gen Comp Endocrinol 114: 80–87
Nishimoto SK, Araki N, Robinson FD, Waite JH (1992) Discovery of bone γ-carboxyglutamic acid protein in mineralized scales. J Biol Chem 267: 11600–11605
Onozato H, Watabe N (1979) Studies on fish scale formation and resorption III: Fine structure and calcification of the fibrillary plates of the scales in *Crassius auratus* (Cypriniformes: Cyprinidae). Cell Tissue Res 201: 409–422
Owan I, Burr DB, Turner CH, Qiu J, Tu Y, Onyia JE, Duncan RL (1997) Mechanotransduction in bone: Osteoblasts are more responsive to fluid forces than mechanical strain. Am J Physiol Cell Physiol 273: C810–C815
Peng Q, Wang Y, Qiu J, Zhang B, Sun J, Lv Y, Yang L (2011) A novel mechanical loading model for studying the distributions of strain and mechano-growth factor expression. Arch Biochem Biophys 511: 8–13
Persson P, Björnsson B. Th, Takagi Y (1999) Characterization of morphology and physiological actions of scale osteoclasts in the rainbow trout. J Fish Biol 54: 669–684
Saito M, Soshi S, Fujii K (2003) Effect of hyper- and microgravity on collagen post-translational controls of MC3T3-E1 osteoblasts. J Bone Miner Res 18: 1695–1705
Sakimura T, Uchida S, Kono Y, Ochiai T, Fujimoto N (2003) Developmental status of aquatic animal experiment facility, aquatic habitat (AQH), for International Space Station. Biol Sci Space 17: 240–241
Searby ND, Steele CR, Globus RK (2005) Influence of increased mechanical loading by hypergravity on the microtubule cytoskeleton and prostaglandin E2 release in primary osteoblasts. Am J Physiol 289: C148–C158
Suda T, Takahashi N, Udagawa N, Jimi E, Gillespie MT, Martin TJ (1999) Modulation of osteoclast differentiation and function by the new members of the tumor necrosis factor receptor and ligand families. Endocr Rev 20: 345–357
Sun X, McLamore E, Kishore V, Fites K, Slipchenko M, Porterfield DM, Akkus O (2012) Mechanical stretch induced calcium efflux from bone matrix stimulates osteoblasts. Bone 50: 581–591
Suzuki N, Hattori A (2002) Melatonin suppresses osteoclastic and osteoblastic activities in the scales of goldfish. J Pineal Res 33: 253–258
Suzuki N, Suzuki T, Kurokawa T (2000) Suppression of osteoclastic activities by calcitonin in the scales of goldfish (freshwater teleost) and nibbler fish (seawater teleost). Peptides 21: 115–124
Suzuki N, Kitamura K, Nemoto T, Shimizu N, Wada S, Kondo T, et al. (2007) Effect of vibration on osteoblastic and osteoclastic activities: Analysis of bone metabolism using goldfish scale as a model for bone. Adv Space Res 40: 1711–1722
Suzuki N, Danks JA, Maruyama Y, Ikegame M, Sasayama Y, Hattori A, et al. (2011) Parathyroid hormone 1 (1–34) acts on the scales and involves calcium metabolism in goldfish. Bone 48: 1186–1193
Takeda H (2008) Draft genome of the medaka fish: A comprehensive resource for medaka developmental genetics and vertebrate evolutionary biology. Dev Growth Differ 50: S157–S166
Tamma R, Colaianni G, Camerino C, Di Benedetto A, Greco G, Strippoli M, et al. (2009) Microgravity during spaceflight directly affects *in vitro* osteoclastogenesis and bone resorption. FASEB J 23: 2549–2554
Tanaka SM, Li J, Duncan RL, Yokota H, Burr DB, Turner CH (2003) Effects of broad frequency vibration on cultured osteoblasts. J Biomech 36: 73–80
Teitelbaum SL (2000) Bone resorption by osteoclasts. Science 289: 1504–1508
Tjandrawinata RR, Vincent VL, Hughes-Fulford M (1997) Vibrational force alters mRNA expression in osteoblasts. FASEB J 11: 493–497
To TT, Witten PE, Renn J, Bhattacharya D, Huysseune A, Winkler C (2012) Rankl-induced osteoclastogenesis leads to loss of mineralization in a medaka osteoporosis model. Development 139: 141–150
Watanabe-Asaka T, Mukai C, Mitani H (2010) Technologies and analyses using medaka to evaluate effects of space on health. Biol Sci Space 24: 3–9
Yoshikubo H, Suzuki N, Takemura K, Hoso M, Yashima S, Iwamuro S, et al. (2005) Osteoblastic activity and estrogenic response in the regenerating scale of goldfish, a good model of osteogenesis. Life Sci 76: 2699–2709
Zylberberg L, Bonaventure J, Cohen-Solal L, Hartmann DJ, Bereiter-Hahn J (1992) Organization and characterization of fibrillar collagens in fish scales in situ and in vitro. J Cell Sci 103: 273–285

(Received July 13, 2012 / Accepted October 20, 2012)